

## Effects of surface states on two-dimensional electron gas in ZnMgO/ZnO heterostructures

Qun Li<sup>1</sup>, Jingwen Zhang<sup>\*,1,2</sup>, Li Meng<sup>1</sup>, and Xun Hou<sup>1,2</sup>

- <sup>1</sup> Key Laboratory for Physical Electronics and Devices of the Ministry of Education and Key Laboratory of Photonics Technology for Information of Shaanxi Province, School of Electronics and Information Engineering, Xi'an Jiaotong University, Xi'an 710049, P. R. China
- <sup>2</sup> ISCAS-XJTU Joint Laboratory of Functional Materials and Devices for Informatics, School of Electronics and Information Engineering, Xi'an Jiaotong University, Xi'an 710049, P. R. China

Received 19 March 2013, revised 28 September 2013, accepted 11 October 2013 Published online 27 November 2013

Keywords II-IV semiconductors, self-consistent, semiconductor heterostructures, surface states, two-dimensional electron gas

The band profile and electronic properties of Zn-polar ZnMgO/ZnO heterostructures are investigated using self-consistent calculations of the Schrödinger, Poisson, and charge balance equations for 300 K, all based on the assumption that the two-dimensional electron gas (2DEG) originates from donor-like surface states on the ZnMgO (0001) surface. Two models with different surface state distributions are applied to explain the ZnMgO thickness dependence of the 2DEG density. Multi-

subband occupation of the 2DEG is taken into account, and surface states are included using Fermi–Dirac statistics. The polarization charge density at the ZnMgO/ZnO interface and the surface donor energy are added as adjustable fitting parameters to optimize the fits of the two models to experimental data. The fitting results indicate that surface states are more likely to be localized at a single energy level. Lastly, the microscopic origin of the surface states is discussed.

© 2013 WILEY-VCH Verlag GmbH & Co. KGaA, Weinheim

**1 Introduction** Zinc oxide-based materials have become increasingly important in optoelectronic devices operating in the blue and ultraviolet regions, due to the direct ZnO gap of 3.4 eV and the large excitonic ZnO binding energy of 60 meV [1-4]. The high sheet carrier concentration (approximately  $1.0 \times 10^{13} \, \text{cm}^{-2}$ ) and high mobility (approximately  $10^5 \text{ cm}^2 \text{ V}^{-1} \text{ s}^{-1}$ ) of the two-dimensional electron gas (2DEG) in ZnMgO/ZnO heterostructures forecast the prospects for fabricating high-power, high-frequency electronic devices [2, 5-9]. Although significant attention has been given to ZnMgO/ZnO heterostructures, the formation mechanism of the 2DEG at the interface is still under debate. In some heterostructures reported in the literature [6, 10], the ZnMgO and ZnO bulk layers were eliminated as possible sources of the 2DEG, because the 2DEG density was not proportional to the thickness of either layer. Additionally, the carrier densities in undoped ZnMgO and ZnO bulk layers are on the order of  $10^{17}$  and  $10^{16}$  cm<sup>-3</sup> [6], respectively, which are negligible values and are not sufficient for producing a high 2DEG density (up to  $10^{13}$  cm<sup>-2</sup>). Like the AlGaN/GaN 2DEG system, donor-like surface states on the ZnMgO (0001) surface are thought to be the main origin of the 2DEG in Zn-polar ZnMgO/ZnO heterostructures [11–15].

In the research on the 2DEG, various issues remain unsolved, including the energy level position and the distribution and microscopic origin of the surface states. In AlGaN/GaN heterostructures, the single-level surface states are widely used to explain the AlGaN thickness dependence of the 2DEG density and the Fermi-energy pinning [14–16]. Gorden et al. [17] and Miao et al. [18] observed that the Fermi level increased with AlGaN thickness and suggested that the 2DEG originates from continuously distributed surface states on the Ga-polar AlGaN (0001) surface. Chris et al. [19] and Segev et al. [20] stated that the surface state distribution is affected by the growth condition, which is supported by the fact that moderate Ga/N ratios result in single-level surface states; additionally, high Ga/N ratios result in continuously distributed-level surface states. Even for single-level surface states, the reported energy-level position has different values, ranging from 1.0 to

<sup>\*</sup>Corresponding author: e-mail jwzhang@mail.xjtu.edu.cn, Phone: +86 29 8266 4684, Fax: +86 29 8266 4684



1.65 eV [15, 16]. These issues remain unresolved, especially for ZnMgO/ZnO heterostructures. More detailed studies of surface states are necessary to understand the 2DEG formation mechanism for both AlGaN/GaN and ZnMgO/ZnO heterostructures. In this work, we present theoretical studies to understand the effects of surface states on the 2DEG and to extract several properties of the surface states of ZnMgO/ZnO heterostructures.

Here, the Zn-polar ZnMgO/ZnO heterostructure is assumed to be in thermodynamic equilibrium with zero external electric fields; furthermore, the heterostructure consists of a fully strained ZnMgO barrier layer and a fully relaxed ZnO buffer layer on a sapphire substrate. The selfconsistent numerical calculations of the Schrödinger, Poisson, and charge balance equations are carried out for 300 K based on the assumption that the 2DEG originates from donor-like surface states on the ZnMgO (0001) surface. In the calculations, we take into account the multisubband occupation of the 2DEG in the ZnMgO/ZnO heterostructures. The band profile and carrier distribution of the ZnMgO/ZnO heterostructures are investigated based on the single-level surface state model. Within the calculations, the influences of the surface state density and ZnMgO thickness on the 2DEG density are examined. Another surface state type with continuously distributed energy levels in the band gap is also adopted in the calculations for comparison. The calculated results are compared with the experimental data for the selection of a more reliable model and to extract several properties of ZnMgO/ZnO heterostructures, such as the surface state density and polarization charge density at the ZnMgO/ZnO interface. Good agreement is reached between the calculations and experiments by increasing the number of adjustable fitting parameters.

**2 Calculations** In the effective mass approximation, the subbands and wave functions of electrons in the growth direction (along the *c*-axis of the heterostructure) can be determined by the Schrödinger equation,

$$-\frac{\hbar^2}{2m^*}\frac{{\rm d}^2}{{\rm d}z^2}\psi(z) + V(z)\psi(z) = E\psi(z), \tag{1}$$

where  $m^*$ ,  $\psi(z)$ , V(z), and E are the electron effective mass, wave function, potential energy, and electron energy, respectively. The potential energy V(z) is related to the electrostatic potential  $\Phi(z)$  via  $V(z) = -e\Phi(z) + \theta(z)\Delta E_{\rm C}$ , where e is the electronic charge,  $\theta(z)$  stands for the step function, the conduction band discontinuity  $\Delta E_{\rm C}$  at the interface of  ${\rm Zn}_{1-x}{\rm Mg}_x{\rm O}/{\rm ZnO}$  is given as  $0.9 \times \Delta E_{\rm g}$ , and  $\Delta E_{\rm g}$  is the band gap discontinuity of 2.145x eV [12]. The boundary conditions are set as  $\psi=0$  at the two extremes of the calculated region to solve the equation.

In the Zn-polar ZnMgO/ZnO heterostructure, the negative polarization charge is bounded at the ZnMgO surface, while the positive polarization charges are bounded at the ZnMgO/ZnO and ZnO/substrate interfaces due to the

spontaneous and piezoelectric polarization effects. The polarization charge at the ZnO/substrate interface is expected to be screened entirely, or the 2DEG will not be confined at the ZnMgO/ZnO interface [21, 22]. For this reason, charge neutrality should be maintained across the ZnMgO layer and the electron channel region, which can be expressed as

$$\int [\sigma_{\text{Surf}} - \sigma_{\text{Tp}} + \sigma_{\text{Ip}} - n_{\text{S}}(z) + \sigma_{\text{ZnMgO}}(z)] dz = 0,$$
(2)

where  $n_{\rm S}(z),~\sigma_{\rm Surf},~\sigma_{\rm Tp},$  and  $\sigma_{\rm Ip}$  are the electron density, ionized surface donor density, the polarization charge density at the surface of ZnMgO, and polarization charge density at the interface of the ZnMgO/ZnO heterostructure, respectively. Considering the effects of spontaneous and piezoelectric polarization in the ZnMgO/ZnO heterostructure, the net polarization charge density  $\sigma_{Ip}$  at the interface is  $0.024x\,\mathrm{C\,m^{-2}}$  for Mg composition x [23], and the spontaneous polarization of ZnO is 0.054 C m<sup>-2</sup> [24]. The polarization charge density at the surface of ZnMgO is  $\sigma_{\rm Tp} = -0.054 - 0.024 x\,{\rm C\,m}^{-2}$ , because the total polarization charge must maintain electric neutrality. The ionized residual donor density  $\sigma_{\rm ZnMgO}(z)$  in the ZnMgO layer is approximately  $10^{17}\,{\rm cm}^{-3}$  in an unintentionally doped ZnMgO/ZnO heterostructure, while the residual donors in the ZnO are ignored. The  $n_S(z)$  and  $\sigma_{ZnMgO}(z)$  are bulk-like terms, but other charge terms in Eq. (2) are assumed to be  $\delta$ functions. Note that the ionized sheet donor density  $(\sigma_{\text{Surf}} + \sigma_{\text{ZnMgO}} \cdot d)$  should first compensate  $(\sigma_{\text{Tp}} - \sigma_{\text{Ip}})$ before forming 2DEG, where d is the thickness of the ZnMgO layer; if not, the charge neutrality condition cannot be maintained.

All mentioned charge components are included in the Poisson equation to yield the electrostatic potential  $\Phi$ ,

$$\frac{\mathrm{d}}{\mathrm{d}z} \left[ -\varepsilon(z) \frac{\mathrm{d}}{\mathrm{d}z} \Phi(z) \right] = \sigma_{\mathrm{Surf}} - \sigma_{\mathrm{Tp}} + \sigma_{\mathrm{Ip}} - n_{\mathrm{S}}(z) + \sigma_{\mathrm{ZnMgO}}(z), \tag{3}$$

where  $\varepsilon(z)$  is the dielectric constant. Using Fermi–Dirac statistics [17, 25], the ionized surface donor density is given by

$$\sigma_{\text{Surf}} = \frac{N_{\text{sd}}}{1 + 2\exp\frac{E_{\text{F}} - E_{\text{D}}}{k_{\text{B}}T}},\tag{4}$$

where  $E_{\rm D}$  is the energy-level of the surface donors, measured from the conduction band edge  $(E_{\rm C})$ ,  $N_{\rm sd}$  is the matching surface donor density,  $k_{\rm B}$  is the Boltzmann constant, and T is the temperature. In the calculations,  $N_{\rm sd}$  and  $\sigma_{\rm ZnMgO}$  are treated as adjustable fitting parameters. The Fermi level,  $E_{\rm F}$ , can be determined from Eq. (2). To solve the Poisson equation, two boundary conditions are employed, namely, the electrostatic potential at the ZnMgO/ZnO interface is zero, and the electrostatic field inside the ZnO layer is zero.

Tampo et al. [12] have reported a constant surface potential  $\varphi$  (i.e. the difference between  $E_{\rm C}$  and  $E_{\rm F}$  at the surface) of approximately 0.8 eV in ZnMgO/ZnO heterostructures for Mg compositions ranging from 0.12 to 0.42. The authors attributed the constant surface potential to the presence of high-density surface states at 0.8 eV below  $E_{\rm C}$ . In our single-level model,  $E_{\rm D}$  is also set to 0.8 eV below  $E_{\rm C}$ , in accordance with the report by Tampo et al.

Taking into account the individual contributions of all subbands, the electron distribution function  $n_S(z)$  can be expressed as [25]

$$n_{\rm S}(z) = \frac{m^* k_{\rm B} T}{\pi \hbar^2} \sum_{i} \ln \left[ 1 + \exp\left(\frac{E_{\rm F} - E_i}{k_{\rm B} T}\right) \right] |\psi_i(z)|^2, \tag{5}$$

where  $E_i$  and  $\psi_i(z)$  are the electron energy and wave function of the *i*-th subband, respectively.

To solve the equations, an initial guess for the potential energy V(z) is substituted into Eq. (1) to obtain the electron energy  $E_i$  and wave function  $\psi_i(z)$  of the i-th subband. The Fermi level  $E_{\rm F}$  is determined from Eq. (2). Consequently, the electron distribution  $n_{\rm S}(z)$  is calculated using Eq. (5) and then is substituted into Eq. (3) to yield the electrostatic potential  $\Phi(z)$ ; as a result, a new potential energy V(z) is obtained. The new V(z) is substituted into Eq. (1) for the next iteration until a self-consistent solution is reached. If the final potential energy V(z) for a given ZnMgO thickness is obtained, it can be used to obtain an initial V(z) for a larger ZnMgO thickness by extrapolating the obtained V(z) of the ZnMgO layer, which is an effective method for determining an approximate initial V(z), allowing the calculation to converge quickly.

## 3 Results and discussion

## 3.1 ZnMgO/ZnO conduction band profile Figure 1 presents the calculated ZnMgO/ZnO conduction band profile and electron distribution for Mg composition x = 0.37, based on the single-level model. Ten electronic subbands are taken into account in the calculations. As shown in Fig. 1, the calculated conduction band profile in ZnMgO exhibits a linear variation with the distance from the ZnMgO surface, implying that the effect of low-density residual donors in ZnMgO is negligible. The large conduction band discontinuity $\Delta E_{\rm C}$ , along with the strong polarization effects, imposes a strong confinement on the 2DEG, leading to a narrow electron distribution over several nanometres in the growth direction. The average distance from the ZnMgO/ZnO interface of the 2DEG is 3.2 nm for a 10-nm-thick layer of ZnMgO and decreases to 2.6 nm for 20nm-thick ZnMgO, indicating that the 2DEG is pushed to the ZnMgO/ZnO interface by a stronger local electric field, which is induced by the higher 2DEG density. The decreasing average distance will increase the alloy disorder and interface roughness scatterings [26]. These effects will

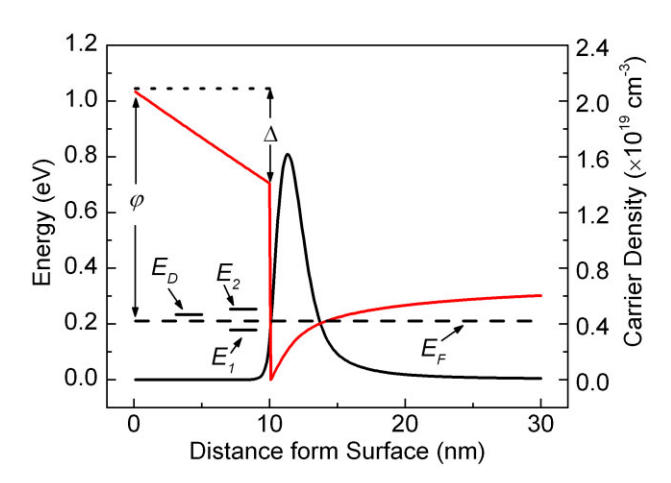


**Figure 1** The calculated conduction band profile and spatially distributed density of the 2DEG for Mg composition x = 0.37 and T = 300 K with a 10-nm-thick ZnMgO layer, based on the single-level model. The  $N_{\rm sd}$  and  $\sigma_{\rm ZnMgO}$  in ZnMgO are assumed to be  $7 \times 10^{13} \, {\rm cm}^{-2}$  and  $1 \times 10^{17} \, {\rm cm}^{-3}$ , respectively.

play important roles in the electronic transport of the 2DEG at low temperatures.

Subband occupation is determined by the 2DEG density and temperature. When the electron density in a 2DEG system exceeds a certain value, higher subbands become occupied. As the temperature decreases, the electrons will transfer from the higher subbands to the ground subband, as dictated by Fermi–Dirac statistics. Lastly, nearly only the ground subband is occupied at a temperature of several Kelvins. For the 2DEG density  $n_{\rm S}=4.9\times10^{12}\,{\rm cm}^{-2}$  given in Fig. 1, 83.1 and 9.5% of the electrons, respectively, occupy the ground subband  $E_1$  and the second subband  $E_2$  at 300 K. When the temperature drops to 4 K, more than 97% of the electrons occupy the ground subband, approaching the electric quantum limit. Han et al. [27] observed the occupation of two-subbands via Shubnikov–de Haas (SdH) oscillation measurements.

3.2 2DEG density and surface potential Figure 2 shows the dependence of the calculated 2DEG density on the ZnMgO thickness for Mg composition x = 0.37, based on the single-level model. The 2DEG cannot be formed until the  $N_{\rm sd}$  exceeds  $3.4 \times 10^{13}$  cm<sup>-2</sup>, because the electrons released from the surface states are attracted by the positive polarization charges at the ZnO/substrate interface until they are neutralized. Then, the 2DEG density increases rapidly with the  $N_{\rm sd}$ . However, when the  $N_{\rm sd}$  is larger than  $4 \times 10^{13} \,\mathrm{cm}^{-2}$ , the 2DEG density is no longer sensitive to further increases in this value. For values of  $N_{\rm sd}$  larger than  $4 \times 10^{13} \,\mathrm{cm}^{-2}$ , the 2DEG density increases rapidly with ZnMgO thickness when the ZnMgO exceeds the critical thickness (i.e. the smallest thickness at which the 2DEG forms). As the ZnMgO thickness exceeds 10 nm, the 2DEG density tends to saturate, due to the restriction of the  $\sigma_{\text{ID}}$ . However, for values of  $N_{\rm sd}$  smaller than  $4 \times 10^{13} \, {\rm cm}^{-2}$ , the saturated 2DEG density is restricted by  $N_{\rm sd}$  and not  $\sigma_{\rm Ip}$ .



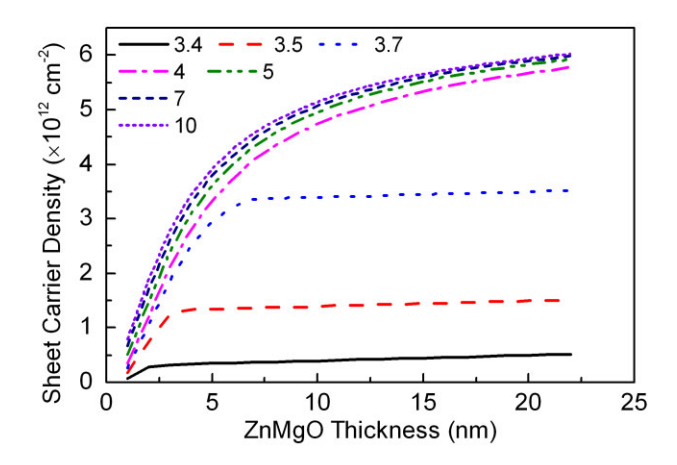


**Figure 2** The dependence of the calculated 2DEG density on the ZnMgO thickness for Mg composition x = 0.37 at 300 K with varying surface state densities. The  $\sigma_{\rm ZnMgO}$  is assumed to be  $1 \times 10^{17} \, {\rm cm}^{-3}$ .  $N_{\rm sd}$  in the legend is in units of  $\times 10^{13} \, {\rm cm}^{-2}$ .

Figure 3 shows the dependence of the 2DEG density on the ZnMgO thickness for Mg composition x=0.37 at 300 K. In addition to the single-level model, a distributed-level model is also adopted in the comparison calculations. In the distributed-level model, the surface donors are assumed to be evenly and continuously distributed between conduction and valence bands, and the surface donor density  $N_{\rm sd}$  is defined as the number of surface donors per unit area and unit energy. Employing Eq. (4),  $\sigma_{\rm Surf}$  is given by integrating over the surface level  $E_{\rm D}$ . It is found that the experimental saturated 2DEG density  $5.9 \times 10^{12} \, {\rm cm}^{-2}$  is close to  $\sigma_{\rm Ip} = 0.024 x/e = 5.6 \times 10^{12} \, {\rm cm}^{-2}$ . Both calculated results, based on the single- and distributed-level models, have similar ZnMgO thickness dependences.

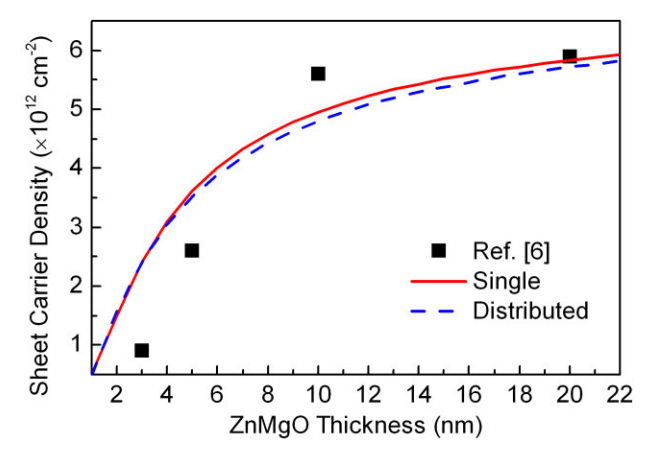


**Figure 3** The dependence of the 2DEG density on the ZnMgO thickness for Mg composition x = 0.37 at 300 K. The solid line corresponds to the single-level model with  $N_{\rm sd} = 7 \times 10^{13} \, {\rm cm}^{-2}$  and  $\sigma_{\rm ZnMgO} = 1 \times 10^{17} \, {\rm cm}^{-3}$ . The dashed line corresponds to the distributed-level model with  $N_{\rm sd} = 4.2 \times 10^{13} \, {\rm cm}^{-2} \, {\rm eV}^{-1}$  and  $\sigma_{\rm ZnMgO} = 1 \times 10^{17} \, {\rm cm}^{-3}$ . The filled squares represent the experimental data from Ref. [6].

For a truly undoped heterostructure in which  $\sigma_{Z_nM_0O}$ = 0, the 2DEG density is restricted by the polarization charge density  $\sigma_{\rm Ip} = 0.024 x\,{\rm C\,m^{-2}}$  at the ZnMgO/ZnO interface if the surface state density is sufficiently large. The saturated 2DEG density is proportional to the Mg composition with a slope of approximately 0.024/e = 1.50 $\times 10^{13}$  cm<sup>-2</sup>. This value is smaller than the experimental values  $(1.83 - 1.98) \times 10^{13} \text{ cm}^{-2}$  [10], perhaps because of the presence of residual donors in the heterostructures and an underestimated value of  $\sigma_{\mathrm{Ip}}.$  If the ZnMgO layer is highly doped, the electrons in the 2DEG may primarily originate from the residual donors in ZnMgO, and the 2DEG density will be proportional to the ZnMgO thickness rather than the Mg composition. Tampo et al. [28] reported a constant 2DEG density with varying Mg compositions, implying that the electrons in the 2DEG may primarily originate from the residual donors in ZnMgO.

Figure 4 shows the dependence of the calculated surface potential height on the ZnMgO thickness for Mg composition x = 0.37, based on the two surface state models. The theoretical data are obtained from the same calculations in Fig. 3. For the single-level model, the calculated surface potential is pinned around the surface donor level, which is set to  $0.8\,\mathrm{eV}$  below  $E_\mathrm{C}$ , and the slight increase corresponds to the process of surface state ionization. With increasing ZnMgO thickness, the gradually screened polarization charge decreases the electrostatic field in the ZnMgO layer, offsetting the increases of the potential difference  $\Delta$ across the ZnMgO layer and causing the  $\Delta$  to approach a constant value. However, the variation of  $E_{\rm F}$  is negligible compared to the  $\Delta$  [12], and the  $\Delta E_{\rm C}$  is determined only based on the Mg composition x. For this reason, the surface potential  $\varphi = \Delta + \Delta E_{\rm C} - E_{\rm F}$  (see Fig. 1) is essentially pinned at the surface states. As the surface state density increases, the variation of the surface potential decreases. In comparison, the surface potential, calculated by the distributed-level model, varies over a larger range, because

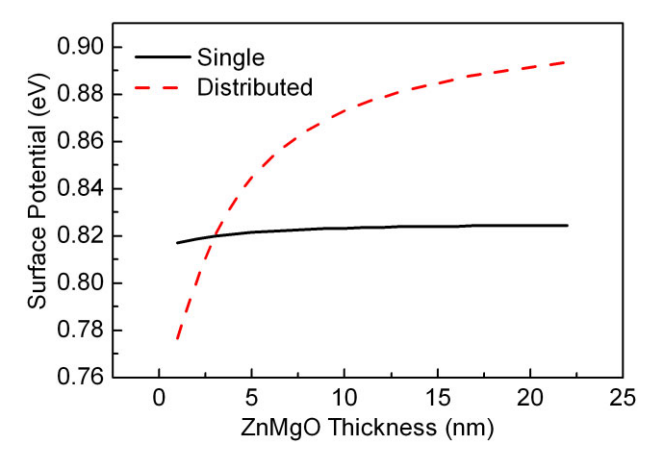


**Figure 4** The dependence of the surface potential on the ZnMgO thickness for Mg composition x = 0.37 at 300 K. The solid and dashed lines correspond to the single- and distributed-level models, respectively.

the lower surface state density is insufficient to pin the surface potential.

**3.3 Optimized model fits** The polarization behaviors of ZnO and ZnMgO are still under discussion. For example, the spontaneous polarization of ZnO is reported in the range of  $0.032-0.057 \,\mathrm{C}\,\mathrm{m}^{-2}$  [23, 24, 29]. The uncertainty in the polarization will significantly affect the precision of associated calculations. In Fig. 3, the deviation of the calculations from the experimental values is readily apparent. More specifically, the calculated critical ZnMgO thickness is smaller than that of the experimental values, and the increase of the calculated 2DEG density at smaller ZnMgO thicknesses is not as sharp as that obtained in the experiments. To optimize further the fitting results of the two models, the surface donor energy  $E_D$  and polarization charge density  $\sigma_{Ip}$  are treated as two adjustable fitting parameters in addition to the  $N_{\rm sd}$  and  $\sigma_{\rm ZnMgO}$ . Figure 5 shows the optimized fit of each model to the experimental data.

As shown in Fig. 5 (the solid line), the optimized fit of the single-level model is in excellent agreement with the experimental data. The fitted values of  $E_{\rm D}$ ,  $\sigma_{\rm Ip}$ , and  $\sigma_{\rm ZnMgO}$  are respectively, 1.15 eV, 0.049x C m<sup>-2</sup>, and 2 × 10<sup>17</sup> cm<sup>-3</sup>; these values are larger than the corresponding parameter values for the original fit shown in Fig. 3 (the solid line), but the fitted  $N_{\rm sd}$  of 4 × 10<sup>13</sup> cm<sup>-2</sup> is smaller than that for the original fit. These changes in the four parameter values

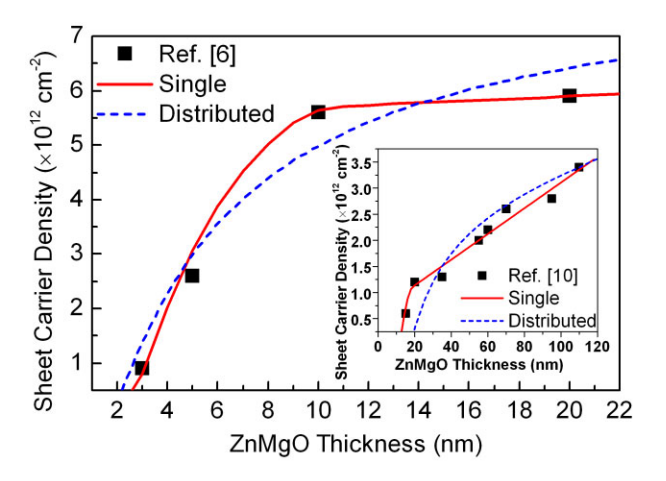


**Figure 5** The dependence of the 2DEG density on the ZnMgO thickness for Mg composition x = 0.37 at 300 K. The solid line corresponds to the single-level model with  $E_{\rm D} = 1.15\,{\rm eV}$ ,  $\sigma_{\rm Ip} = 0.049x\,{\rm C\,m^{-2}}$ ,  $\sigma_{\rm ZnMgO} = 2\times10^{17}\,{\rm cm^{-3}}$  and  $N_{\rm sd} = 4\times10^{13}\,{\rm cm^{-2}}$ , and the dashed line corresponds to the distributed-level model with  $\sigma_{\rm Ip} = 0.035x\,{\rm C\,m^{-2}}$ ,  $\sigma_{\rm ZnMgO} = 1\times10^{17}\,{\rm cm^{-3}}$  and  $N_{\rm sd} = 3.5\times10^{13}\,{\rm cm^{-2}}\,{\rm eV^{-1}}$ . The filled squares are the experimental data from Ref. [6]. The inselt is an additional fit to the experimental data from Ref. [10]. The solid line in the inset corresponds to the single-level model with  $E_{\rm D} = 1.15\,{\rm eV}$ ,  $\sigma_{\rm Ip} = 0.049x\,{\rm C\,m^{-2}}$ ,  $\sigma_{\rm ZnMgO} = 2.5\times10^{17}\,{\rm cm^{-3}}$  and  $N_{\rm sd} = 3.45\times10^{13}\,{\rm cm^{-2}}$ , and the dashed line corresponds to the distributed-level model with  $\sigma_{\rm Ip} = 0.030x\,{\rm C\,m^{-2}}$ ,  $\sigma_{\rm ZnMgO} = 2.1\times10^{17}\,{\rm cm^{-3}}$  and  $N_{\rm sd} = 2.5\times10^{13}\,{\rm cm^{-2}}\,{\rm eV^{-1}}$ .

enable the accurate fit of the single-level model to the experimental data. In this electronic structure, the larger  $E_D$ and  $\sigma_{Ip}$  result in a larger critical ZnMgO thickness and a more rapid increase in the  $n_S$  at smaller ZnMgO thicknesses, respectively, as shown in Fig. 5 (the solid line). The lower density surface donors with  $N_{\rm sd} = 4 \times 10^{13} \, {\rm cm}^{-2}$ completely depleted at a ZnMgO thickness of approximately 10 nm due to the more rapid increase in the  $n_S$ ; as a result, electrons are no longer supplied to the 2DEG, resulting in a plateau-like saturation behavior of  $n_S$  above 10 nm, as shown in Fig. 5. The contribution of the evenly distributed residual donors in ZnMgO is negligible compared with the effect of the surface donor ionization below 10 nm but leads to a slight linear increase of the  $n_S$  above 10 nm. The slope of the linear region of the  $n_{\rm S}$  is equivalent to the  $\sigma_{\rm ZnMgO}$ . All features of the optimized fit of the single-level model give excellent agreement between the calculated and experimental values. The four fitting parameters have different effects on the  $n_S$ behavior and jointly contribute to a significant improvement in the optimized fit of the single-level model.

The optimized fit of the distributed-level model with more adjustable fitting parameters is also performed for comparison. Through a process of trial and error, as shown in Fig. 5 (the dashed line), the optimized fit of the distributed-level model is found to be in good agreement with the experimental data at smaller ZnMgO thicknesses, but fails to accurately reproduce the saturation behavior of the  $n_{\rm S}$ . The distributed-level model cannot predict the plateau-like saturation behavior of the  $n_{\rm S}$ , because the continuously distributed surface donors cannot be depleted.

The two models are also fitted to another experimental data set with Mg composition  $x\!=\!0.15$ . It can be seen from the inset of Fig. 5 that the single-level model fits the experimental data better than the distributed-level model. For each fit of both experimental data sets, the distributed-level model cannot accurately fit the experimental variations of the  $n_{\rm S}$  by adding adjustable fitting parameters, as in the case of the single-level model. Accordingly, the single-level model is more reliable than the distributed-level model.

3.4 Microscopic origin of the surface states For wurtzite ZnO, Kresse et al. [30] stated that triangular reconstructions were more favorable to occur than Zn vacancies or O adatoms on the Zn-polar ZnO (0001) surface. However, Ding and Wang [31] observed surface reconstructions only on the non-polar ZnO  $(0\bar{1}11)$  surface, while Zn vacancies and a random outward displacement of the top Zn ions occurred on the Zn-polar ZnO (0001) surface, based on high-resolution transmission electron microscopy studies. Lin and Hsieh [32] carried out a tight-binding theory analysis to investigate the electronic structure of ZnO and suggested that the dangling cation (Zn) bonds resulted in surface states close to the conduction band minimum, while the dangling anion (O) bonds gave rise to the surface states near the middle of the band gap. According to these studies, the surface donor states are more likely to originate from



the dangling bonds of cations (Zn or Mg). The surface state density on the order of  $10^{13}$  cm $^{-2}$ , which was extracted from the experimental data fitting, represents 1% or less of the areal density of atoms on the surface, implying a low density of cation dangling bonds. In this case, the dilute dangling bond states are isolated from each other, preventing coupling between dangling bonds. Therefore, the surface states have equivalent energy, which is consistent with the single-level model we suggested.

Although the microscopic origin of surface states on Zn-polar ZnMgO/ZnO (0001) surfaces requires additional experiments and theoretical support, the surface states giving rise to the origin of 2DEG are able to explain a wide range of experimental observations, such as the critical ZnMgO thickness, the saturated 2DEG density, and the dependence of the 2DEG density on the ZnMgO thickness. A 2DEG can also be formed in O-polar ZnO/ZnMgO heterostructures consisting of a strained ZnO layer on a relaxed ZnMgO layer [2, 7]. This structure can be viewed as an inverted Zn-polar ZnMgO/ZnO heterostructure with the substrate as a passivation layer. Similar calculations can be applied to the O-polar ZnO/ZnMgO heterostructure.

**4 Conclusions** We investigated the band profile and the ZnMgO thickness dependence of the 2DEG density for ZnMgO/ZnO heterostructures via self-consistent calculations. The approach was based on the assumption that the 2DEG originates from donor-like surface states. When using the fixed polarization charge density at the ZnMgO/ZnO interface and a fixed value of the surface donor energy, the single- and distributed-level models predicted similar ZnMgO thickness dependences of the 2DEG densities, but neither model was able to accurately fit the experimental data. After adding the two parameters as adjustable fitting parameters for further optimization of the fitting results of both models, the single-level model was found to be more reliable and to fit the experimental data better than the distributed-level model. The discussion on the microscopic origin of surface states also supports the singlelevel model.

**Acknowledgments** This work was support by the National Natural Science Foundation of China under Grant Nos. 61176018 and 60876042 and the National High Technology Research and Development Program of China (863 Program) under Grant No. SQ2013GX04D00825.

## References

- [1] Ü. Özgür, Y. Alivov, C. Liu, A. Teke, M. Reshchikov, S. Doğan, V. Avrutin, S-J. Cho, and H. Morkoç, J. Appl. Phys. **98**, 041301 (2005).
- [2] K. Koike, K. Hama, I. Nakashima, G. Takada, M. Ozaki, K. Ogata, S. Sasa, M. Inoue, and M. Yano, Jpn. J. Appl. Phys. 43, L1372 (2004).
- [3] J. Ye, S. Gu, F. Li, S. Zhu, R. Zhang, Y. Shi, Y. Zheng, X. Sun, G. Lo, and D. Kwong, Appl. Phys. Lett. 90, 152108 (2007).

- [4] S. Su, Y. Lu, Z. Zhang, C. Shan, B. Yao, B. Li, D. Shen, J. Zhang, D. Zhao, and X. Fan, Appl. Surf. Sci. 254, 7303 (2008).
- [5] H. Tampo, H. Shibata, K. Matsubara, A. Yamada, P. Fons, S. Niki, M. Yamagata, and H. Kanie, Appl. Phys. Lett. 89, 132113 (2006).
- [6] H. Tampo, H. Shibata, K. Maejima, A. Yamada, K. Matsubara, P. Fons, S. Kashiwaya, S. Niki, Y. Chiba, and T. Wakamatsu, Appl. Phys. Lett. 93, 202104 (2008).
- [7] A. Tsukazaki, A. Ohtomo, T. Kita, Y. Ohno, H. Ohno, and M. Kawasaki, Science 315, 1388 (2007).
- [8] K. Koike, I. Nakashima, K. Hashimoto, S. Sasa, M. Inoue, and M. Yano, Appl. Phys. Lett. 87, 112106 (2005).

15213951, 2014, 4, Downloaded from https://onlinelibrary.wiley.com/doi/10.1002pssb.201349107 by CAS-XIAN INSTITUTION OPTICS PRECISION MECHANICS, Wiley Online Library on [09/11/0225]. See the Terms

on Wiley Online Library for rules of use; OA articles are governed by the applicable Creative Common

- [9] S. Akasaka, A. Tsukazaki, K. Nakahara, A. Ohtomo, and M. Kawasaki, Jpn. J. Appl. Phys. 50, 080215 (2011).
- [10] J. Ye, S. Pannirselvam, S. Lim, J. Bi, X. Sun, G. Lo, and K. Teo, Appl. Phys. Lett. 97, 111908 (2010).
- [11] H. A. Chin, I. C. Cheng, C. I. Huang, Y. R. Wu, W. S. Lu, W. L. Lee, J. Z. Chen, K. C. Chiu, and T. S. Lin, J. Appl. Phys. 108, 054503 (2010).
- [12] H. Tampo, H. Shibata, K. Maejima, T. W. Chiu, H. Itoh, A. Yamada, K. Matsubara, P. Fons, Y. Chiba, and T. Wakamatsu, Appl. Phys. Lett. 94, 242107 (2009).
- [13] M. Higashiwaki, S. Chowdhury, M. S. Miao, B. L. Swenson, C. G. Van de Walle, and U. K. Mishra, J. Appl. Phys. 108, 063719 (2010).
- [14] J. Ibbetson, P. Fini, K. Ness, S. DenBaars, J. Speck, and U. Mishra, Appl. Phys. Lett. 77, 250 (2000).
- [15] B. Jogai, J. Appl. Phys. 93, 1631 (2003).
- [16] K. S. Lee, D. H. Yoon, S. B. Bae, M. R. Park, and G. H. Kim, ETRI J. 24, 270 (2002).
- [17] L. Gordon, M. S. Miao, S. Chowdhury, M. Higashiwaki, U. K. Mishra, and C. G. Van de Walle, J. Phys. D: Appl. Phys. 43, 505501 (2010).
- [18] M. Miao, J. Weber, and C. Van de Walle, J. Appl. Phys. 107, 123713 (2010).
- [19] G. Chris, d. W. Van, and S. David, J. Appl. Phys. 101, 081704 (2007).
- [20] D. Segev and C. G. Van de Walle, J. Cryst. Growth 300, 199 (2007).
- [21] G. Koley and M. Spencer, Appl. Phys. Lett. 86, 042107 (2005).
- [22] H. Tokuda, J. Yamazaki, and M. Kuzuhara, J. Appl. Phys. 108, 104509 (2010).
- [23] A. Malashevich and D. Vanderbilt, Phys. Rev. B 75, 045106 (2007).
- [24] S. Massidda, R. Resta, M. Posternak, and A. Baldereschi, Phys. Rev. B **52**, R16977 (1995).
- [25] B. Jogai, J. Appl. Phys. 91, 3721 (2002).
- [26] A. Gold, Appl. Phys. Lett. 96, 242111 (2010).
- [27] K. Han, N. Tang, J. D. Ye, J. X. Duan, Y. C. Liu, K. L. Teo, and B. Shen, Appl. Phys. Lett. 100, 192105 (2012).
- [28] H. Tampo, K. Matsubara, A. Yamada, H. Shibata, P. Fons, M. Yamagata, H. Kanie, and S. Niki, J. Cryst. Growth 301, 358 (2007).
- [29] Y. Noel, C. Zicovich-Wilson, B. Civalleri, P. D'arco, and R. Dovesi, Phys. Rev. B 65, 014111 (2001).
- [30] G. Kresse, O. Dulub, and U. Diebold, Phys. Rev. B. 68, 245409 (2003).
- [31] Y. Ding and Z. L. Wang, Surf. Sci. 601, 425 (2007).
- [32] K. F. Lin and W. F. Hsieh, J. Phys. D: Appl. Phys. 41, 215307 (2008).